Nanoscale

Accepted Manuscript

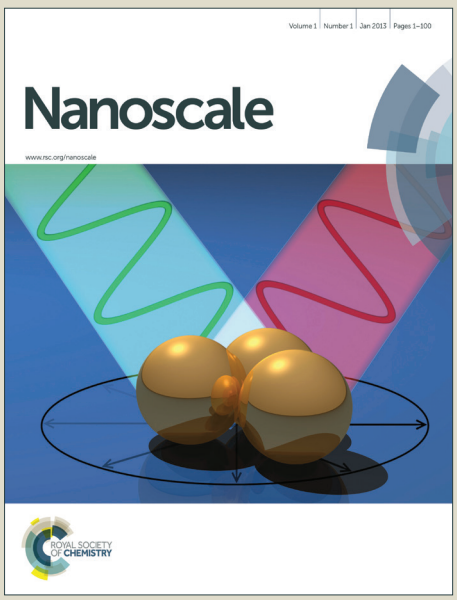

ROYAL SOCIETY OF CHEMISTRY

www.rsc.org/nanoscale

Nanoscale

ARTICLE

Frequency-dependent learning achieved using semiconducting polymer/electrolyte composite cells

Received 00th January 20xx,
Accepted 00th January 20xx

DOI: 10.1039/x0xx00000x

www.rsc.org/

W.S. Dong,[a,b] F. Zeng,[a,b]*, S.H. Lu, [a,b] A. Liu,[a] X.J. Li, [a,b] and F. Pan[a]*

Frequency-dependent learning has been achieved using semiconducting polymer/electrolyte composite cells. The cells composed of polymer/electrolyte double layers realized the conventional spike-rate-dependent plasticity (SRDP) learning model. These cells responded to depression at low-frequency stimulation and to potentiation at high-frequency stimulation and presented long-term memory. The transition threshold ϑ_m from depression to potentiation varied depending on the previous stimulations. Nano structure resembling bio-synapse in its transport passages was demonstrated and a random channel model was proposed to describe ionic kinetics at the polymer/electrolyte interface during and after stimulations with various frequencies, accounting for the observed SRDP.

1. Introduction

Currently, materials and devices with synaptic-like behaviours are attracting widespread attentions in the fields of materials, informatics and neuroscience.[1-6] The hope is that they will become the critical elements of neuromorphic circuits contributing to brain-like computation, which would overcome the shortcomings of current computer architecture and reduce energy consumption. This issue proceeds quickly and extensively. Many material systems (e.g., memristors) have been used to emulate synaptic functions and realize principal learning models, such as Hebbian learning, spike-rate-dependent plasticity (SRDP) and spike-timing-dependent plasticity (STDP). [7-12] Recent study confirmed that the artificial neuromorphic system constructed by the memristors can be trained and operated effectively.[13] Moreover, it has been found that the memristor not only offer resistance change but also internal variable to exhibit Ca^{2+} like dynamics encoding timing information.[14] Thus, finding system owing internal variable emulating ion flux in bio-synapse would be an effective way prompting application of artificial synapse.

Doping into organic semiconductor usually involves oxidation and reduction of π electrons, during which the inserted countra-ions are used for electrical balance.[15] This process is reversible because the matrix could be inserted by either cation or anion, depending on the input polarity. The amount and rate of countra-ions become state variable. We therefore supposed to use semiconducting polymer/electrolyte hetero-junction to emulate synaptic plasticity. This consideration was first identified in our recent research on pulse response in a Pt/poly(3-hexylthiophene-2,5-diyl) (P3HT)/polyethylene oxide (PEO)+Li^+/Pt device.[16] We adopted a conventional measurement paradigm in neuroscience to study pulse responses (see measurement protocol in Figure S1), [17, 18] in which the pulses of fixed strength and width were used as action potential, after which the stimulation strength could be encoded and handled in circuits constructed with this type of device as well as in neural circuits. This device behaved selectively with regard to the pulse frequency, i.e., exhibiting depression under low-frequency stimulation (LFS) but potentiation under high-frequency stimulation (HFS), and might be used as a band filter.[19]

However, long-term memory (LTM) or long-term plasticity (LTP) was not observed in the previous work so the device cannot be used to mimic spike-rate-dependent plasticity (SRDP) learning model though the responses *vs* stimulations frequency approximated each other in shape.[16] SRDP is one of the important learning models proposed initially to resolve the problems of selectivity and stability of synaptic plasticity met in the Hebbian learning model.[17, 20, 21] Besides the frequency selectivity mentioned above, the weight modification in SRDP has a transition threshold from depression to potentiation, which could be modified depending on the previous experience. We supposed that frequency selectivity with LTM would be achieved if the states of the semiconducting polymer could be modified and conserved.

The feasibility of the foregoing considerations was demonstrated in this study. Both LTM and learning effects have been accomplished. We replaced the P3HT used in the previous study with poly[2-methoxy-5-(2-ethylhexyloxy)-1,4-

[a] *Laboratory of Advanced Materials (MOE), School of Materials Science and Engineering, Tsinghua University, Beijing 100084, People's Republic of China.*
[b] *Center for Brain Inspired Computing Research (CBICR), Tsinghua University, Beijing 100084, People's Republic of China*
*Corresponding Author
† Footnotes relating to the title and/or authors should appear here.
Electronic Supplementary Information (ESI) available: [details of any supplementary information available should be included here]. See DOI: 10.1039/x0xx00000x

phenylenevinylene] (MEH-PPV) and constructed devices with MEH-PPV/PEO+Li^+ double layers as intermediate media (Fig. 1). The MEH-PPV layer can be either n-doped or p-doped.[22, 23]

2. Experimental

Poly[2-methoxy-5-(2-ethylhexyloxy)-1,4-phenylenevinylene](MEH-PPV), polyethylene oxide (PEO, MW = 100000), lithium trifluoromethanesulfonate ($LiCF_3SO_3$) and cyclohexanone were purchased from Sigma-Aldrich Co. Ltd. and used as is. MEH-PPV was fully dissolved into cyclohexanone to obtain a solution of 8 mg/mL, then stirred at 38℃ for 24 h. PEO and $LiCF_3SO_3$ were dissolved into deionized water with the matching principle of (EO):Li^+=16:1. A silicon substrate with 100 nm previously deposited Pt film was used as the bottom electrode (BE). Fabrication of MEH-PPV/PEO+Li^+ double layer: 3 µL MEH-PPV solution was spin coated at 2000 rpm for 70 s and then baked at 50 ℃ for 6 h. Then, 3 µL aqueous solution of the PEO and $LiCF_3SO_3$ was drop-casted on the MEH-PPV film and baked at 65℃ for 20 min. The thickness of the MEH-PPV film was approximately 90 nm, and the thickness of the PEO+Li^+ film was about 8 µm. All of the steps of preparing polymer and electrolyte were completed in a glovebox filled with nitrogen. After the preparation of the composite, Pt top electrodes (TE) with a diameter of 300 µm and a thickness of 80 nm were deposited by electron beam evaporation through a shadow mask.

The electrical measurements were conducted on a semiconductor analysis platform (B1500A, Agilent) composed of an arbitrary function generator (B1530, Agilent). The BE was grounded during the measurement in ambient environment. The schematic of the measurement protocol was plotted and described in detail in Fig. S1. Both of the rectangular and triangular stimulations were consisted of 40 spikes in a train, regardless of frequencies. Raman spectra were obtained on an HR-800 Raman system, in which a 633 nm HeNe laser was used as the excitation source. Scanning electrical microscopy images were obtained using a LEO-1530 scanning electron microscope.

3. Results and discussion

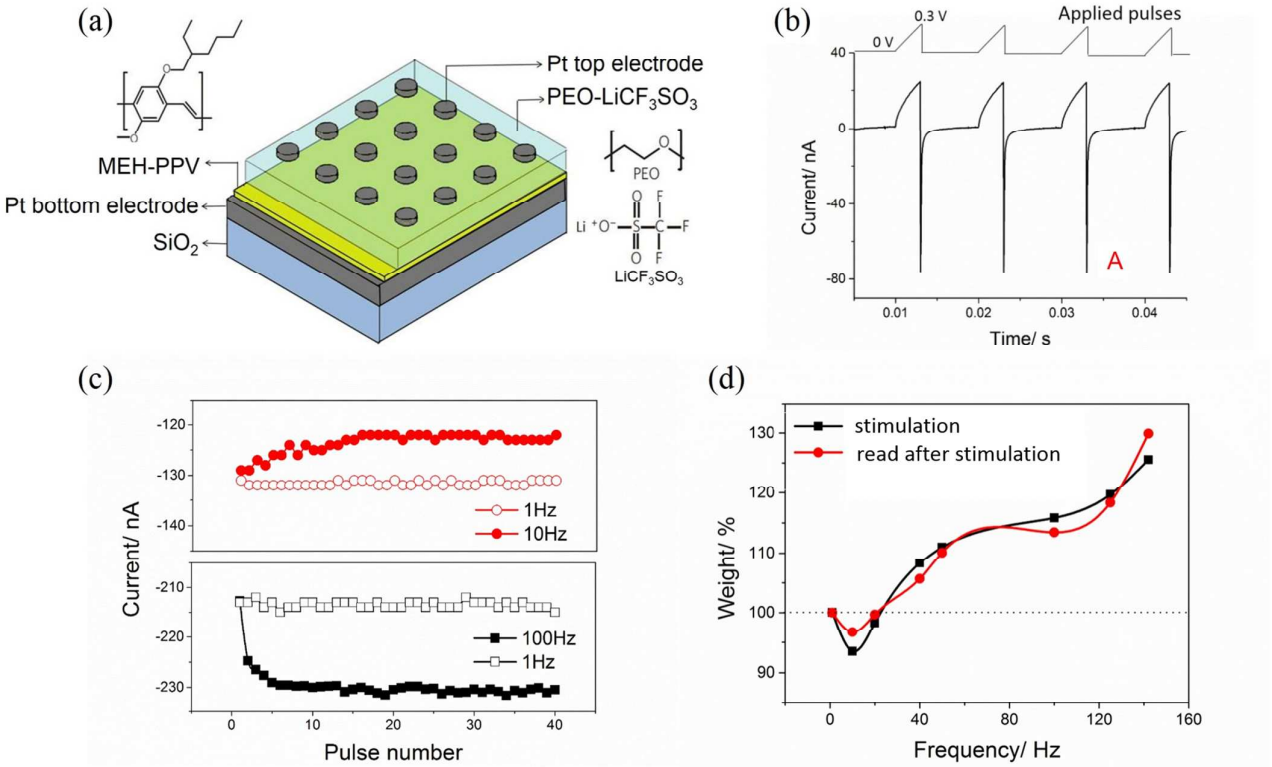

Fig. 1 Responses to pulse frequency and corresponding weight modifications obtained by using a train of stimulations with 0.3V triangular pulses. (a) Schematic of device structure. (b) Responses to a train of pulses with amplitude 0.3 V and width 3 ms. Point A indicates EPSC or IPSC. (c) Response varied with pulse number. The sequences were 1 Hz→10 Hz (upper panel) and 1 Hz→100 Hz, respectively. (d) Weight modifications for the device with MEH-PPV/PEO double layer. The last ten I_A in (c) were averaged to get error bars, which were smaller than the symbols in both curves. Black-square line in (d) stands for responses to stimulation with various frequencies (1-142 Hz). Red-dotted line in (d) stands for weights of responses to baseline frequency (1 Hz) 5 min after stimulation.

Responses to pulse frequency and their weight modifications are illustrated in Figs. 1b-d. A train of pulses, with amplitude of 0.3 V and width of 3 ms, was applied to the device (Fig. 1b). The discharging peak (I_A) was used as the excitatory postsynaptic current (EPSC) or inhibitory postsynaptic current (IPSC), related to the release probability

of a neurotransmitter in a bio-synapse.[17, 18, 24] The values of I_A varied with the pulse number and stabilized at last (Fig. 1c). Apparently, I_A in response to a 10 Hz pulse was smaller than the previous 1 Hz (upper panel in Fig. 1c), while that in response to a 100 Hz pulse was bigger than the previous 1 Hz (lower panel in Fig. 1c). This comparison indicates clearly that the device was adaptive to the type of stimulation and was selective with regard to the input frequency. Importantly, these two properties are intrinsic properties of bio-synapses.[4] We used I_A *(f=1 Hz)* as the baseline, calculated the weight modification using the formula of W= I_A *(f)* /I_A *(f=1 Hz)*, and plotted the weight modifications in Fig. 1d. The use of 1 Hz baseline was due to the reason that we did not observed weight modification in the 1 Hz→1 Hz→1 Hz measurement protocol. Thus, we used 1 Hz for convenience to design experiment and measurement procedures. Using equilibrium condition without stimulation could be one option for selecting baseline state. However, there are usually random signals passing through a synapse in the resting state. Two principal aspects of the frequency responses could be concluded from Fig. 1.

First, the device with a MEH-PPV/PEO+Li^+ double layer responded to depression (W < 100) from 10 to 20 Hz but potentiation (W > 100) when the frequency was higher than 20 Hz (line made of black-square in Fig. 1d). Second, weight modification varied with the same trend in responses to both stimulations and 1 Hz read pulses 5 min later (red-dotted line in Fig. 1d), which suggested the devices could retain their memory or synaptic plasticity in the longer term. Moreover, similar frequency selectivity was also obtained if the pulse was 0.1 V rectangular as shown in Fig. S2d. The difference was that the absolute values were lower than that in Fig. 1d, suggesting the dependence of frequency selectivity on input form.

The transient response, i.e. charge and discharge with device impedance, leaky resistance, and parasitic capacitance are critical for high speed and low current measurement and especially using the discharge current. We compared the pulse responses of a pure capacitor, a resistor and their RC circuits connected in parallel and in series with that of our device in Fig. S2. We found that the measurement circuitry had not parasitic capacitance. The MEH-PPV/PEO-Li^+ hetero-junction and PEO-Li^+ are intrinsically capacitive as well as a RC circuit connected in series. Nyquist impedance spectra (Fig. S3) also confirmed that the MEH-PPV/PEO-Li^+ hetero-junction was ionic transport in the frequency range lower than 200 Hz. The pulse responses was not frequency selective for the circuit constructed by a resistor and a capacitor connected in series. The pulse responses of the capacitor indicated that there is not leaky resistance existing in the measurement circuitry. The surface and lateral side of the device were unlike to provide leaky resistance because the PEO layer was ionic conductive. If the ions appeared in the surface and lateral side, they were oxidized immediately. Therefore, the frequency selectivity observed in Fig. 1 should come from modulation of ionic migration across the polymer/electrolyte interface.

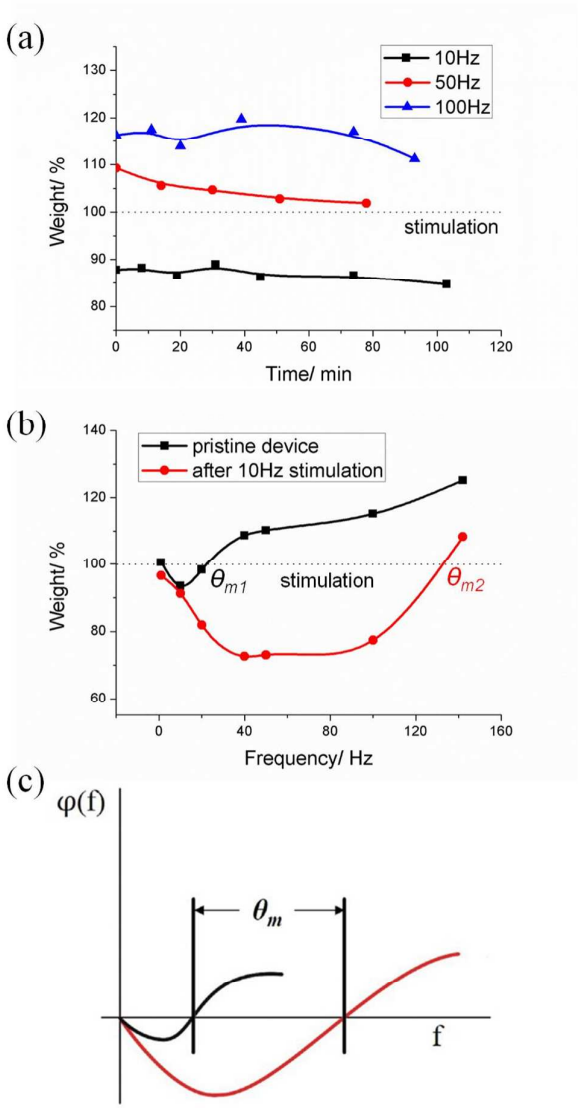

Fig. 2. Long-term synaptic plasticity and sliding thresholds obtained by using a train of stimulations with 0.3 V triangular pulses. (a) Weight modifications obtained 100 to 360 min after stimulations. (b) Weight modifications of responses to stimulations measured from pristine devices (line consisting of black-square) and from the devices stimulated using 10 Hz frequency 5 min before (red dotted line). (c) Schematics of BCM learning model. Modification function ϕ(f) depresses at a low firing rate f but potentiates at a high firing rate. The threshold ϑ_m indicates the transition from depression to potentiation. It can be moved owing to the modifications of the initial states.

The next issue raised naturally in this work was if the LTM or LTP could be obtained. As a triangular wave approximates the action potential in shape, we adopted a triangular wave with an amplitude of 0.3 V and a width of 3 ms to study the LTM or LTP. The loaded frequency sequence was 1 Hz (the baseline frequency) → n Hz (n > 1, stimulations)→ 1 Hz → 1 Hz → 1 Hz → 1 Hz. LTM could be observed clearly in Fig. 2a. The device stimulated at 10 Hz pulses was depressed after 20

min, and its weight became even lower after 100 min. The device stimulated at 100 Hz was still potentiated after 100 min. There were a common decay for the three frequencies, which might be due to the aging effect during the measurement process in air. The LTP/LTM of a specific stimulation was measured on an individual device with the measurement protocol. One device corresponded to one stimulation except the measurements of Fig. 2b and Fig. S4. Therefore, the LTP/LTM was not claimed to be achieved simultaneously on one device. We did not find that the weight modifications were affected by the neighbouring device on the same piece (see Table S1).

Furthermore, it is interested to know how the device responded under two consecutive different sets of stimulations. The device was firstly loaded with 10 Hz pulse and then added stimulation with other frequencies after 5 min. Fig. 2b shows that the stimulated device resulted in depression (weight < 100) until the second stimulation was enhanced to 120 Hz. The threshold ϑ_m of the transition from depression to potentiation was increased from 20 Hz to approximately 120 Hz, suggesting a sliding threshold ϑ_m as shown in Fig. 2c. Secondly, the device was loaded with higher frequency pulses (i.e. 50Hz) and followed by the stimulations with other frequencies. A potentiation at all frequencies was only observed, but a left threshold shift was not observed (Fig. S4).

The results in upper and lower panel of Fig. 1c were obtained by using different devices. Their current difference for the same 1 Hz stimulation is caused by device variation due to varied thickness and roughness, which was induced by preparing the PEO layer using the drop-casting technique. The frequency responses in Fig. 1d and Fig. 2b were achieved from different devices to avoid a history effect generating after the previous measurement. Device-to-device variations did exist due to the great fluctuations of thickness and surface roughness. This could be confirmed by the results in Table S1, and might give small plasticity change. Improvement in fabrication to obtain smooth surface might be helpful to reduce the device-to-device variations and get large weight modification values.

The results in Figs. 1 and 2 demonstrated that our device displayed SRDP resembling the BCM learning rule proposed by Bienenstock, Cooper and Paul Munro.[17, 20, 25] An early study had found that the Hebbian learning model encountered a problem in physiology: the synaptic weight would increase in an unlimited manner with stimulation and exhibited no selectivity to stimulations.[20, 26, 27] A learning model was subsequently proposed by Cooper, Liberman and Oja (CLO) to solve the selectivity problem first,[20, 27] which was supported by the discovery of depression at low frequencies of prolonged modest rise after the delivery of [Ca^{2+}] in experiments.[28] A threshold (ϑ_m) was then introduced in the CLO learning model to distinguish which signals can be responded to by neurons ($f > \vartheta_m$) and which ones cannot ($f < \vartheta_m$). Later, the BCM learning model established that the threshold ϑ_m would be moved after the system had been modified (Fig. 2c),[17, 20] i.e., it is sliding to stabilize the system. In our case, the resting device responded to depression below 20 Hz and with potentiation higher than 40 Hz so that the threshold ϑ_m was in the range of 20 to 40 Hz. If the device was subjected to 10 Hz stimulation first, ϑ_m was enhanced greatly to approximately 120 Hz.

A difference should be noticed. By common sense about BCM theory, after a period of increased synaptic activity, the threshold will slide to right (higher frequency), promoting synaptic depression. Similarly, after a period of decreased activity, the threshold will slide to left, promoting synaptic potentiation and it will be easier to enhance synaptic weight with lower-frequency spikes. However, the ϑ_m value of our device moved to right after 10 Hz pulse. The complex structure and ion dynamics of our devices may lead to what is observed. More experiments and measurement routines are needed to confirm if our device is consistent with the BCM learning rule.

Our previous study did not obtain LTM,[16] though the weight-frequency curves resembled that in BCM theory. However, the previous observation could be employed in band filtering or synaptic computation.[19] Many studies in neuroscience have found that frequency selectivity occurred *in vivo* without LTP, which was regarded as an important signal handling method but not related to memory and learning.[29] Our current study made a major breakthrough in which not only was LTM or LTP realized, but also a sliding threshold was observed. These features are consistent with BCM theory, i.e., SRDP,[20] which is an important learning protocol widely studied. At present stage, the works of artificial synapses using memristor usually simulate SRDP and the other important learning rule, i.e., STDP, which had been cared about in our previous works.[8, 10, 16] However, we focused our attention on the observed SRDP and its mechanism in this study.

We have known that the frequency selectivity disappeared when the pulse amplitude was lower than the inflection point, i.e., 0.1 V. An important issue might be how to effectively select input pulse or signal depending on the background in biology. The endurance of the cells could be referred to the measurement of LTM. From the stand point of retention, the cells could effectively display the same properties in the second measurement in a week as shown in Fig. S5. Many studies in neuroscience calculate weight modification by integrating the EPSC, in which the integrated weight is usually consistent with the weight calculated from the discharging peak, especially for short term plasticity.[18] We also calculated the weight by integrating the discharging process of the last pulse response and plotted the results in Fig. S6. It is clearly that the integrated weights varied in the same trend with the peak weights for the stimulation processes.

In order to understand the mechanism of the observed SRDP learning behaviour, we need to know the electronic properties and microstructure in depth. First, we notice that the results in Figs. 1d & e imply a common ionic kinetics of ion migration existing in both the double layer. Direct current-voltage (I-V) properties were then examined for the

device with an MEH-PPV/PEO+Li^+ double layer (Figs. 3a & b). An inflection point at approximately 0.1 V appeared in the I-V curves during the loading process with a positive bias (Fig. 3a). Significant negative differential resistance (NDR) and a substantially higher conductance could be observed if the bias was swept in a cycle of 0 V → 2 V → 0 V → -2 V → 0 V. These results suggested that the initial state of MEH-PPV was different from the initial state of the previously used P3HT.[16] The initial state of MEH-PPV might be n-doped (or Li^+ doped) during the preparation process. The initially doped Li ions could weaken the doping rate driven by the positive bias, resulting in an inflective point at quite a small voltage (~0.1 V in Fig. 3a). If the bias was swept in the negative direction, some of the Li ions would be driven back to the PEO+Li^+ layer. Thus, NDR occurred easily owing to the hysteretic properties of ions when the bias returned to a positive value, which was also confirmed by the results measured using various sweep cycles, as shown in Fig. S7.

The assumption about initial Li-doping at the interface was further confirmed by using Raman spectra to check the initial state of MEH-PPV. As shown in Fig. 3c, the peak of MEH-PPV at 1585 cm^{-1}, which represents the C-C stretch of benzene ring, moved to 1581 cm^{-1} after being covered by the PEO+Li^+ layer. This red shift also existed for the mixture of MEH-PPV and PEO+Li^+ and the suggested reduced vibration energy of MEH-PPV. The red shift should result from the decreased π-π* energy gap of carbon on the benzene ring caused by n-doping (i.e., Li^+ doping) of MEH-PPV.[15, 30, 31] We have repeated Raman measurements for more than three times and confirm this result, though these variations values were small. Therefore, interface diffusion between MEH-PPV and PEO+Li^+ occurred initially according to the Raman spectra and the various DC I-V curves.

We further examined the microstructures of both MEH-PPV and the electrolyte film. Spherulitic textures of PEO+Li^+ were found in optical images, indicating a mixed structure of crystalline lamellae and amorphous materials between lamellae.[32-34] Ions could migrate in the channel with nano-scale of the amorphous phase. Cross-sectional images of the devices (Figs. 4a & b) gave us direct analogies to the structure of bio-synapses. Fig. 4a shows that MEH-PPV (approximately 100 nm) did not contact PEO+Li^+ entirely or was not infiltrated completely with PEO+Li^+. A bundle of PEO fibres corresponding to a molecular backbone (Fig. 4b), which was analogous to those reported,[35] was oriented perpendicularly to the MEH-PPV layer. A similar image could also be observed for the mixture of MEH-PPV and PEO+Li^+, i.e., the PEO nanofibres with a diameter of approximately 10 nm nearly intersected with the MEH-PPV matrix (Fig. 4c). It has been proved that ion conduction in PEO is confined within the chain fold region and guided by the crystalline lamellae, while the amorphous space between lamellar provided nano-scale passageway for ions to get through.[34, 35] So Li^+ ions can be supposed to transport within those nano-channels formed by well oriented PEO matrix (Fig. 4b), the phenomena of which resembles the neurotransmitter passing from pre- to post-synaptic neuron (Figs. 5a & b).

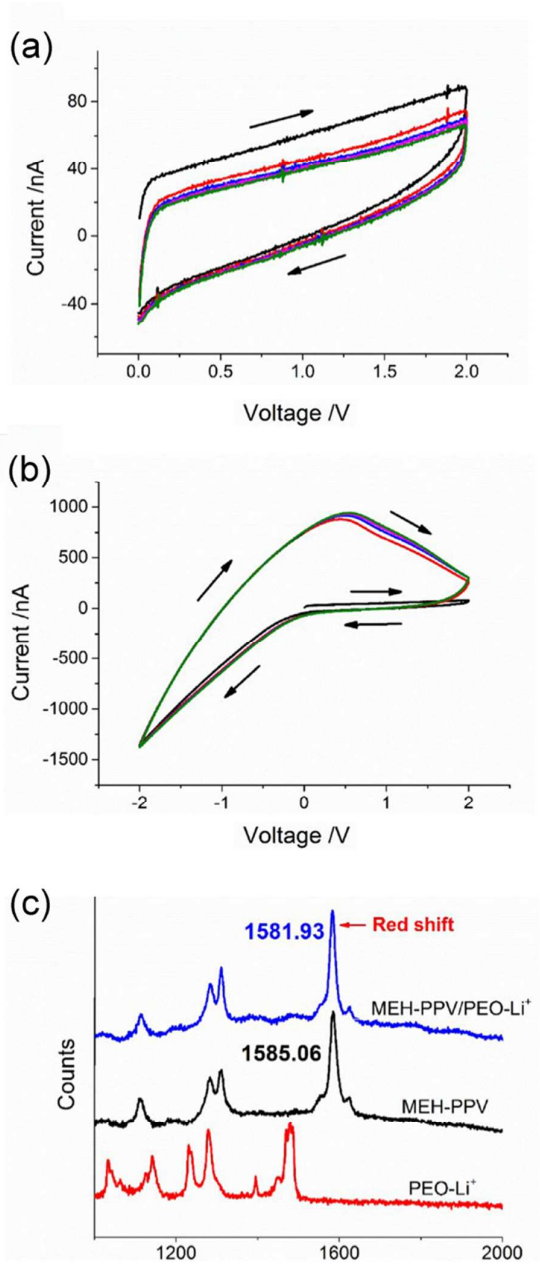

Fig. 3. Direct current-voltage (I-V) curves and Raman spectra of MEH-PPV/PEO composites. (a) I-V curves measured in a sweep cycle of 0-2 V. (b) I-V curves measured in a sweep cycle of 0→ 2→0→-2→0 V. (c) Raman spectra of MEH-PPV and PEO.

The above analyses in electrical properties (including impedance) and structure determined that the system was ionic transportation in the experimental frequency range. Ionic flux is the state variable as well as that in bio-synapse. The state variable, such as the postsynaptic Ca^{2+} concentration in a synapse, will be overlapped if the input frequency increased to the extent that the consecutive pulses

arrive before the Ca^{2+} concentration decays to the resting value.[36, 37] It is apparently to see that the weight potentiates with the input frequency, which has appeared also in memristor characterized by the state variable: temperature.[14, 38] At this category, the state variable could be encoded by the spike timing. However, the depression at LFS is hard to be understood or may be contradictory to potentiation in HFS. We analyzed the typical responses to the stimulation frequencies, i.e., 10 Hz (depression) and 100 Hz (potentiation), and to the following 1 Hz read pulse in depth, and extracted timing constants by fitting the last discharging processes and listed them in Table I. Accordingly, we tried to demonstrate the intrinsic mechanism of the observed SRDP using a phenomenological mode in the following section.

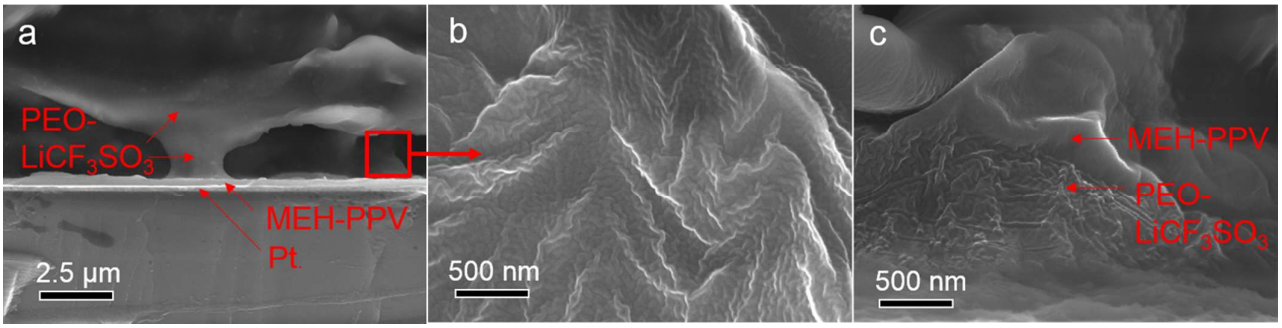

Fig. 4. Microstructures of MEH-PPV/PEO composites. Cross-sectional images of (a) and (b) MEH-PPV/PEO double layer, and (c) MEH-PPV/PEO mixture.

Apparently, the discharging processes of the MEH-PPV/PEO cells were quite different from the typical capacitor, resistor and R+C circuit (see Fig. S2 and Fig. S8). Neither the total discharging process can be fitted by using a simple exponent decay curve. The discharging process of the MEH-PPV/PEO cells mainly composed of a rapid range and a slow range (Fig. S8). The current in the former was high and decayed quickly, while that in the later was low and decayed slowly. It suggested that the ionic flux experienced a rapid decay and an interaction to delay this decay simultaneously after the input pulse ended. The later might come from the interaction between the ions and the MEH-PPV or PEO chains.[15, 39, 40]

Similar discharging process can be found in the responses of memristor with initially faster decay,[14] of which the time constant was also quiet larger than that of electron in a pure capacitive system as well as that in our cells. However, there is not attention on its variations. Considering oxygen vacancy was the principal resistive switching mechanism,[14] we thought that ionic migration or interfacial de-polarization account for the rapid range of the discharging process in both our cell and memristor.[41-43] The system state was determined by the rapid range. We fitted the data within 1 ms by using a simple exponent decay function and got results well consistent with the experimental with parameters listed in Table I.

The apparent differences between the stimulations of 10 Hz (LFS) and 100 Hz (HFS) can be observed in Table I. The initial y0 decreased under & after depression stimulation (10 Hz), and the time constant (54 to 57 μs) increased in the contrast. However, the initial y0 increased under & after potentiation stimulation (100 Hz), and the time constant decreased in the contrast (104 to 95 μs).

Table I. Time constant of discharging process extracted from numeric fitting formula of y = A1*exp(-x/t1) + y0. The 0.3 triangular pulse was used.

Frequency /Hz	1	10	1	1	100	1
y0	3.45E-9	3.17E-9	3.24E-9	3.74E-9	4.92E-9	4.38E-9
A1	1.21E+17	8.91E+15	5.97E+16	9.2E+5	3.66E+6	3.55E+6
t1	5.43 E-5	5.69E-5	5.5E-5	1.07E-4	9.52E-5	9.53E-5

It is known that the lithium ions' lowest energy positions are at particular positions inside the PEO backbone helix,[44] and the energy of other positions near the central axis of backbone helix is ~0.4 eV more than the lowest energy.[45] This suggested that lithium ions do not actively hop in room temperature but could move directionally under the stimulation of applied bias. Therefore, we could establish a synaptic-like structural model (Fig. 5c and Fig. 6) in which numerous ion channels (i.e., nanofibres) were inserted into the MEH-PPV layer (Figs. 5a & b). The latter was doped initially during the preparation process (denoted by three or five deep grey dots in the uppermost panel in Fig. 5c). The MEH-PPV layer and PEO+Li^+ layer were denoted by orange colour and grey colour respectively.

It is also known that ions are excited stochastically in the electrolyte under moderate electrical loading,[39, 40, 46-48] which kind of random excitation should exist in our PEO nanofibres. Another element of randomness was the fluctuation of the initial doping content in polymer along each channel due to the randomness in the preparation process. Those channels with either low interfacial doping would be easily conductive, which is defined as active channels C_a. The other channels are defined as dormant channels C_d. The C_a channels are denoted by three grey dots and the C_d channels are denoted by five grey dots (the 1st panel in Fig. 5c). The number of C_a is assumed n_a and the active ions in one C_a channel is assumed N_a. Both C_a and N_a could be modified depending on external electrical field, temperature and doping effect in MEH-PPV. The total ions influencing weight modifications are initially $n_a \times N_a$, which may varied after pulse interaction. We referred the weight data obtained by 10 Hz and 100 Hz to

demonstrate the mechanism of depression and potentiation representatively.

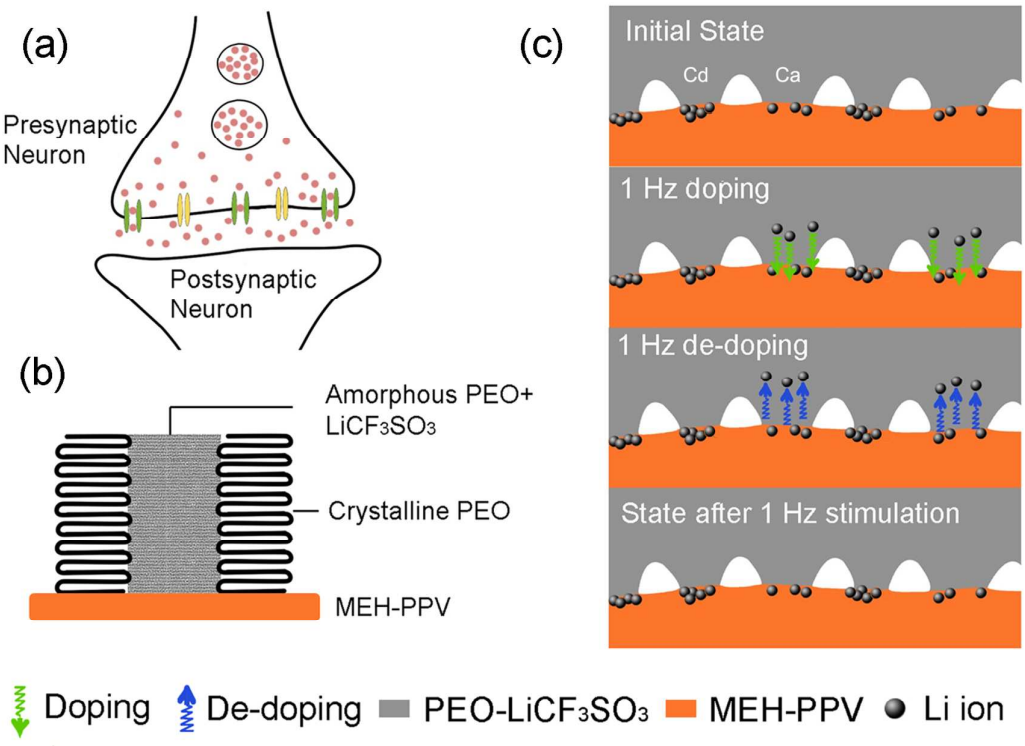

Fig. 5. Mechanism of spike-rate-dependent-plasticity. (a) Schematic of bio- synapse. (b) Schematic of PEO-$LiCF_3SO_3$/MEH-PPV interface structure. (c) Random ionic channel model of 1 Hz (baseline) stimulation. The uppermost and lowest panels: resting state. Numerous ion channels intersected with MEH-PPV, and the ion number doped along individual channel fluctuated in a small range. The intermediate two panels: C_a channel was activated, C_d channel was dormant, N_{doping}^{b} (total ions along green arrows) was compatible with N_{de}^{b} (total ions along blue arrows).

When a small external pulse was added, whether the memory or learning occurred is relative to the ion states at the polymer/electrolyte interface. The baseline frequency normally corresponds to the resting state in neuroscience, in which the system state is not modified. The individual pulse response was fully relaxed under the input with the baseline frequency so that the later pulse did not influence the relaxation response induced from the previous pulse. The ionic migration process under the baseline frequency is shown in Fig. 5c. The doping ions ($N_{doping}^{b}= n_a \times N_a$, 'b' denotes baseline) during the pulse width, which are denoted by summing grey dots along the green arrows in the 2nd panel in Fig. 5c, were consistent with the de-doping ions after a set of pulses ($N_{de}^{b}= N_{doping}^{b}$, total grey dots along the blue arrows in Fig. 5c,). Besides, the values of n_a and N_a are not modified. Therefore, the system could not be modified at its baseline inputs. This is indicated by the total grey dots in the orange layer in the 1st panel that are equivalent to those in the 4th panel in Fig. 5c.

When the frequency was enhanced to a moderate value, i.e., LFS, the neighboring pulses would influence mutually depending on the interval. The 1st panel in Fig. 6a shows that there was a small amount of ions of the discharging after the 1st pulse near the interface just before the 2nd pulse arrived, which stands by a grey cycle at the end of blue arrow. These ions initially were parts of N_a. However, their moments were small and the local heat effect induced by strong ionic flux had dissipated after long term relaxation. The 2nd pulse pushed these ions deeply into the MEH-PPV layer because they are near the interface. The total doping ions along C_a was still N_a and $N_{doping}^{L}= n_a \times N_a$ (the 2nd panel in Fig. 6a, 'L' denotes LFS). However, fewer ions were trapped in the MEH-PPV layer and the recoiling ions were less than N_a during the discharging process after the 2nd pulse. N_{de}^{L} was lower than $n_a \times N_a$ ($\sim N_{doping}^{L}$). This could be supported by the decreased

Nanoscale

ARTICLE

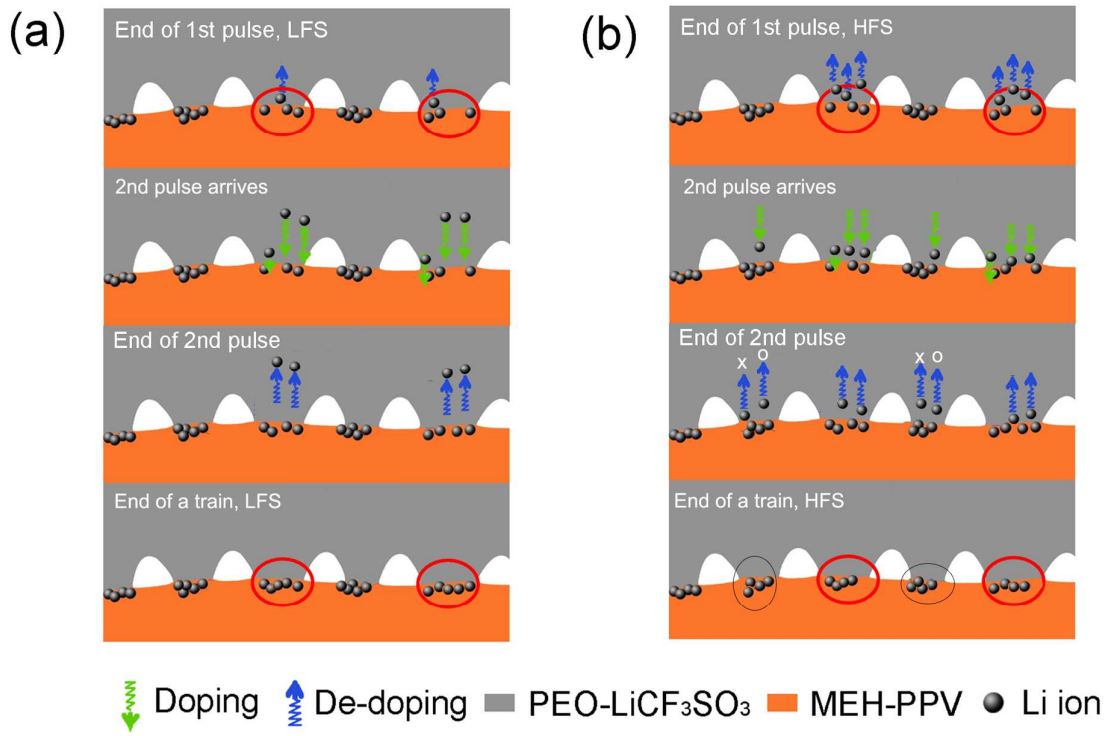

Fig. 6. Schematic of ionic migration under LFS and HFS, respectively. (a) LFS, ~10 Hz. $N_{de}^{L} < N_{doping}^{L}$. The initial state got modified with more trapped ions in MEH-PPV layer. (b) HFS, ~100 Hz. $P_2 > P_1$ channels were activated. $N_{de}^{H} > N_{de}^{b}$, where P_2 was also an activated probability. The initial state got modified by ions dragged back into PEO layer in new activated channels.

discharging peak and elongated discharging time constant for LFS (Table I), and that both the charging peak and discharging peak all decreased slightly (Fig. S9). The state of the 4th panel in Fig. 6a was formed after a train of LFS. The interfacial barrier become stronger due to the trapped ions, which can reduce the external bias allocated on the electrolyte layer. Thus, the active ions N_a' could be lower than N_a and the de-doping strength decreased lastly. Consequently, the weight modification became depression under LFS and the system state was modified in the long term, in which the amount of ions in the polymer layer increased.

When the frequency was enhanced further, i.e., HFS, the interval was so short that the de-doping ions were still near the interface and had moderate kinetic moment (the 1st panel in Fig. 6a). The 2nd pulse arrived before complete relaxation (the 2nd panel in Fig. 6b). Since the ions were aggregated at the interface in instantaneous period and had relative high moment inverse to the electric field, a strong inbuilt electrical field was induced to counteract external field. At this time, the total inbuilt field became larger than or comparable to barrier at the interface and along the neighbouring dormant channels. Thus, some ions owing low energy as the active N_a were be activated and driven to the polymer layer in these initial dormant channels, which is indicated by single green arrow + single grey dots in the 2nd panel in Fig. 6b. Thus, the total doping ions was more than the initial N_a in the initial channel C_a. The heat effects of the previous strong discharging might have auxiliary effect in increasing activated ions because the heat might not have dissipated effectively.[14]

When the 2nd pulse ended, one of possible increase of total de-doping ions (N_{de}^{H}, H stands for HFS) was that the activated ions in the 2nd panel (denoted by 'o') evoked release of an ion not combined tightly with MEH-PPV (denoted by 'x'). Besides, one ion in the previous active channel was trapped in the MEH-PPV layer. Thus, the total de-doping ions (N_{de}^{H}, blue arrows + grey dots) were more than those of the 1st panel in Fig. 6b and then the weight increased. The last state after HFS might be the 4th panel in Fig. 6b, in which the total activated channels increased ($n_a' > n_a$) because the barriers in all

channels became more equally. The active ions in each channels decreased a little ($N_a'<N_a$). However, the total active ions $n_a' \times N_a'$ increased eventually. There is of course a situation in which both n_a' and N_a' increased but less ions staying in the MEH-PPV layer. These categories are consensus with the fitting results in Table I, in which the discharging values increased while the time constant decreased after HFS. Besides, the experimental results in Fig. S9 supported the above suggestions.

The sliding threshold in Fig. 2b can also be understood in above model. Apparently, the state of the 4th panel in Fig. 6a needs high frequency to increase the probability to activate effective ions in the channels, to evoke release of some trapped ions in the MEH-PPV layer, and to arrive the state of the 4th panel in Fig. 6b. Thus the transition threshold ϑ_m from depression to potentiation becomes larger.Besides, we used 50 Hz stimulation before the other stimulations and found that all the weights increased (Fig. S4). The state in the 4th panel in Fig. 6b should be hard to be transformed to the depression state. Decreasing temperature might be a way. Due to the complicated kinetics in organic semiconducting polymer and electrolyte, there might be other routines to explain the observed SRDP. Above model is self-consistent and provides a base for quantitatively studying, analysing and manipulating this SRDP protocol.

These works suggest that large and applicable weight modification would be obtained for either short term or long term plasticity. Using discharging current to determine weight is a great challenge for designing circuit because transient response could be seriously affected by circuit parameter. However, the main problem at present stage is to understand the mechanisms of this type of materials and device definitely. We will establish new circuit designing principal according to these research results. For example, we suggest that using different ions could construct a variety of frequency selectivity. This would become the base of signal handling in network in the future. Printing and electro-spinning beyond the current semiconducting technology would be important techniques to integrate this type of materials and device. Three dimension (3D) neuromorphic network is expectative.

4. Conclusions

In summary, frequency-dependent learning, i.e., the conventional SRDP learning model, has been achieved using semiconducting polymer/electrolyte composite cells. The cells composed of the polymer/electrolyte double layer responded to depression at LFS and to potentiation at HFS and displayed a LTM. The transition threshold ϑ_m from depression to potentiation varied depending on the previous stimulations. On the basis of the analogies between the microstructures of our cells and the bio- synapse, we proposed a random ionic channel model to demonstrate the ionic kinetics at the semiconducting polymer/electrolyte interface and describe the observed SRDP learning process. We thought that such stimulations could modify the initial state of MEH-PPV, which was doped during fabrication. That is, a modified state slowly relaxed, resulting in LTP or LTM and the occurrence of learning. Our results suggested a way to design artificial synapse.

Acknowledgements

This work was supported by National Natural Science foundation of China (Grant Nos. 51371103 and 51231004), National Hi-tech (R&D) project of China (Grant No. 2013AA030801), the Research Project of Chinese Ministry of Education (No 113007A) and Brain Inspired Computing Research, Tsinghua University (20141080934).

Notes and references

1. P. Sheridan and W. Lu, in *Memristor Networks*, eds. A. Adamatzky and L. Chua, Springer, Cham Heidelberg New York Dordrecht London, 2014, p. 129.
2. S. H. Jo, T. Chang, I. Ebong, B. B. Bhadviya, P. Mazumder and W. Lu, *Nano Lett.*, 2010, **10**, 1297-1301.
3. J. J. Yang, D. B. Strukov and D. R. Stewart, *Nature Nanotech.*, 2013, **8**, 13-24.
4. C. Zamarreño-Ramos, L. A. Camuñas-Mesa, J. A. Pérez-Carrasco, T. Timothée Masquelier, T. Serrano-Gotarredona and B. Linares-Barranco, *Frontiers in Neuronscience*, 2011, **5**, 26.
5. Y. C. Yang and W. Lu, *Nanoscale*, 2013, **5**, 10076-10092.
6. T. Ohno, T. Hasegawa, T. Tsuruoka, K. Terabe, J. K. Gimzewski and M. Aono, *Nature Mater.*, 2011, **10**, 591-595.
7. T. Chang, S. H. Jo and W. Lu, *ACS Nano*, 2011, **5**, 7669-7676.
8. S. Z. Li, F. Zeng, C. Chen, H. Liu, G. S. Tang, S. Gao, C. Song, Y. S. Lin, F. Pan and D. Guo, *J. Mater. Chem. C*, 2013, **1**, 5292-5298.
9. Z. Q. Wang, H. Y. Xu, X. H. Li, H. Yu, Y. C. Liu and X. J. Zhu, *Adv. Funct. Mater.*, 2012, **22**, 2759-2765.
10. F. Zeng, S. Z. Li, J. Yang, F. Pan and D. Guo, *RSC Adv.*, 2014, **4**, 14822.
11. W. He, K. J. Huang, N. Ning, K. Ramanathan, G. Q. Li, Y. Jiang, J. Y. Sze, L. P. Shi, R. Zhao and J. Pei, *Sci. Rep.*, 2014, **4**, 4755.
12. L. Q. Zhu, C. J. Wan, L. Q. Guo, Y. Shi and Q. Wan, *Nature Commun.*, 2014, **5**, 3158.
13. P. Prezioso, F. Merrikh-Bayat, B. D. Hoskins, G. C. Adam, K. K. Likharev and D. B. Strukov, *Nature*, 2015, **521**, 61-64.
14. S. Kim, C. Du, P. Sheridan, W. Ma, S. H. Choi and D. W. Lu, *Nano Lett.*, 2015, **15**, 2203-2211.
15. A. J. Heeger, N. S. Sariciftci and E. B. Namdas, *Semiconducting and Metallic Polymers*, Oxford University Press, 2010.
16. F. Zeng, S. H. Lu, S. Z. Li, X. J. Li and F. Pan, *PLoS ONE*, 2014, **9**, e108316.
17. S. M. Dudek and M. F. Bear, *PNAS*, 1992, **89**, 4363-4367.
18. David L. Brody and David T. Yue, *J. Neurosci.*, 2000, **20**, 2480-2494.
19. L. F. Abbott and W. G. Regehr, *Nature*, 2004, **431**, 796.
20. L. N. Cooper and M. F. Bear, *Nature Rev. Neurosci.*, 2012, **13**, 798-810.

21. N. Intrator and L. N. Cooper, *Neural Networks*, 1992, **5**, 3-17.
22. J. Gao, Y. F. Li, G. Yu and A. J. Heeger, *J. Appl. Phys.*, 1999, **86**, 4594.
23. Q. B. Pei, G. Yu, C. Zhang, Y. Yang and A. J. Heeger, *Science*, 1995, **269**, 1086-1088.
24. G. Q. Bi and M. M. Poo, *J. Neurosci.*, 1998, **15**, 10464-10472.
25. G. Rachmuth, H. Z. Shouval, M. F. Bear and C. S. Poon, *PNAS*, 2011, **108**, E1266–E1274.
26. Y. Fregnac and M. Imbert, *J. Physiol.*, 1978, **278**, 27M24.
27. L. N. Cooper, F. Liberman and E. Oja, *Biol. Cybern.*, 1979, **33**, 9-28.
28. M. F. Bear, L. N. Cooper and F. F. Ebner, *Science*, 1987, **237**, 42-48.
29. Z. Rotman, P. Y. Deng and V. A. Klyachko, *J. Neurosci.*, 2011, **31**, 14800 - 14809.
30. Q. Pei, Y. Yang, G. Yu, Y. Cao and A. J. Heeger, *Synthetic Met.*, 1997, **85**, 1229-1232.
31. Z. B. Yu, L. Li, H. E. Gao and Q. B. Pei, *Sci. China Chem,*, 2013, **56**, 1075-1086.
32. Y. W. Kim, W. Lee and B. K. Choi, *Electrochim. Acta*, 2000, **45**, 1473-1477.
33. B. K. Choi and Y. W. Kim, *Mater. Sci. Eng. B*, 2004, **107**, 244-250.
34. Fullerton-Shirey. S.K and J. K. Maranas, *Macromolecules,* , 2009, **42**, 2142-2156.
35. S. Cheng, D. M. Smith and C. Y. Li, *Macromolecules*, 2014, **47**, 3978-3986.
36. S. N. Yang, Y. G. Tang and R. S. Zucker, *J. Neurophysiol.*, 1999, **81**, 781-787.
37. H. Z. Shouval, M. E. Bear and L. N. Cooper, *PNAS*, 2002, **99**, 10831-10836.
38. C. Du, W. Ma, T. Chang, P. Sheridan and D. W. Lu, *Adv. Funct. Mater.*, 2015, **DOI: 10.1002/adfm.201501427**.
39. L. Gitelman, A. Averbuch, M. Nathan, Z. Schuss and D. Golodnitsky, *J. Chem. Phy.*, 2010, **107**, 064318.
40. Y. H. Duan, J. W. Halley, L. Curtiss and P. Redfern, *J. Chem. Phy.* , 2005, **122**, 054702.
41. G. S. Tang, F. Zeng, C. Chen, H. Y. Liu, S. Gao, C. Song, Y. S. Lin, G. Chen and F. Pan, *Nanoscale*, 2013, **5**, 422-428.
42. Z. S. Wang, F. Zeng, J. Yang, C. Chen and F. Pan, *ACS Appl. Mater. & Interfaces*, 2012, **4**, 447-453.
43. Y. C. Yang and W. Lu, *Nanoscale*, 2013, **5**, 10076-10092.
44. P. Johansson, J. Tegenfeldt and J. Lindgren, *Polymer*, 1999 **40**, 4399-4406.
45. P. Johansson, J. Tegenfeldt and J. Lindgren, *Polymer*, 2001 **42**, 6573-6577.
46. D. Bamford, A. Reiche, G. Dlubek, F. Alloin, J.-Y. Sanchez and M. A. Alam, *J. Chem. Phys.*, 2003, **118**, 9420.
47. A. E. Javier, S. N. Patel, D. T. Hallinan Jr., V. Srinivasan and N. P. Balsara, *Angew. Chem. Int. Ed.*, 2011, **50**, 9848 -9851.
48. S. N. Patel, A. E. Javier, G. M. Stone, S. A. Mullin and N. P. Balsara, *ACS Nano*, 2012, **6**, 1589–1600.

1